

Supplementary Figures

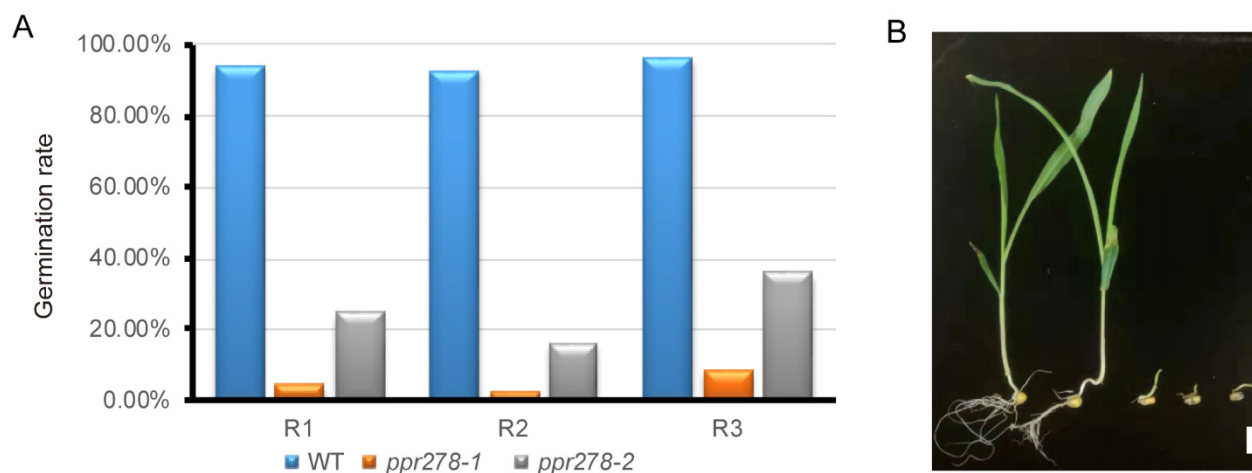


Figure S1. Phenotype of *ppr278* seedlings. **(A)** Analysis of the germination rate of WT and *ppr278-1* and *ppr278-2* mutant seeds. R1, R2, and R3 represent replicates 1, 2, and 3, respectively. **(B)** Seedling development status from heterozygous ears (*PPR278/ppr278-1* and *PPR278/ppr278-2*) 10 days after sowing (DAS), from left to right: normal kernel of *PPR278-1* and normal kernel of *ppr278-2*, *ppr278-1*, *ppr278-1*, and *ppr278-2* mutants. Bar = 10 mm.

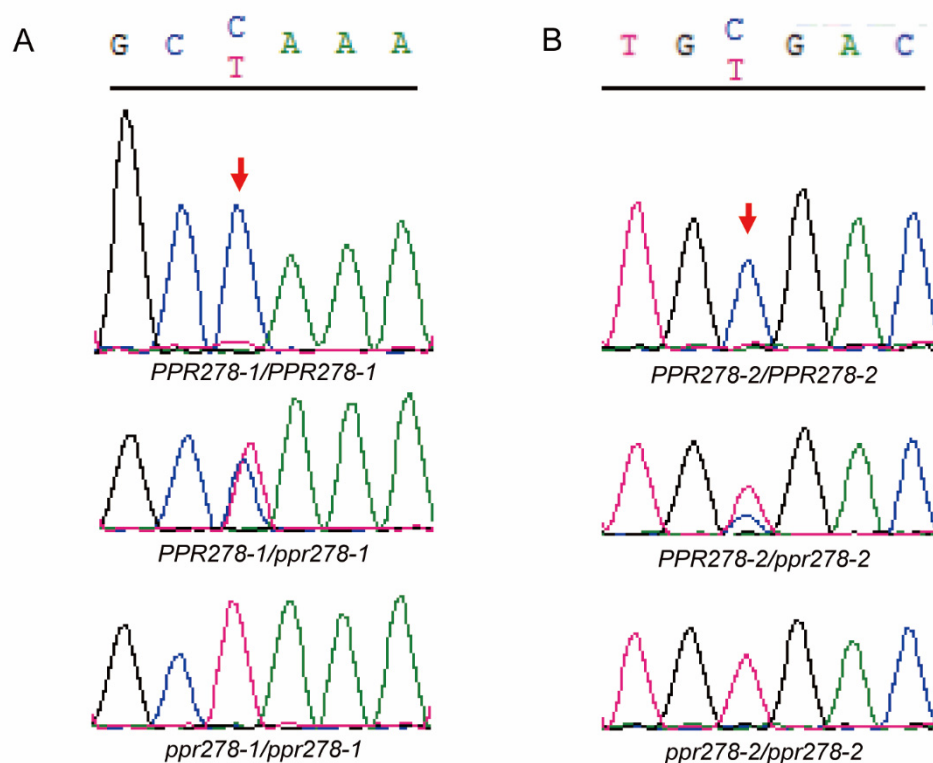


Figure S2. Co-isolation test of *ppr278*. **(A,B)**. Two pairs of mutant site-spanning primers were designed to test the relationship between the genotype and phenotype in *ppr278-1* and *ppr278-2* mutants.

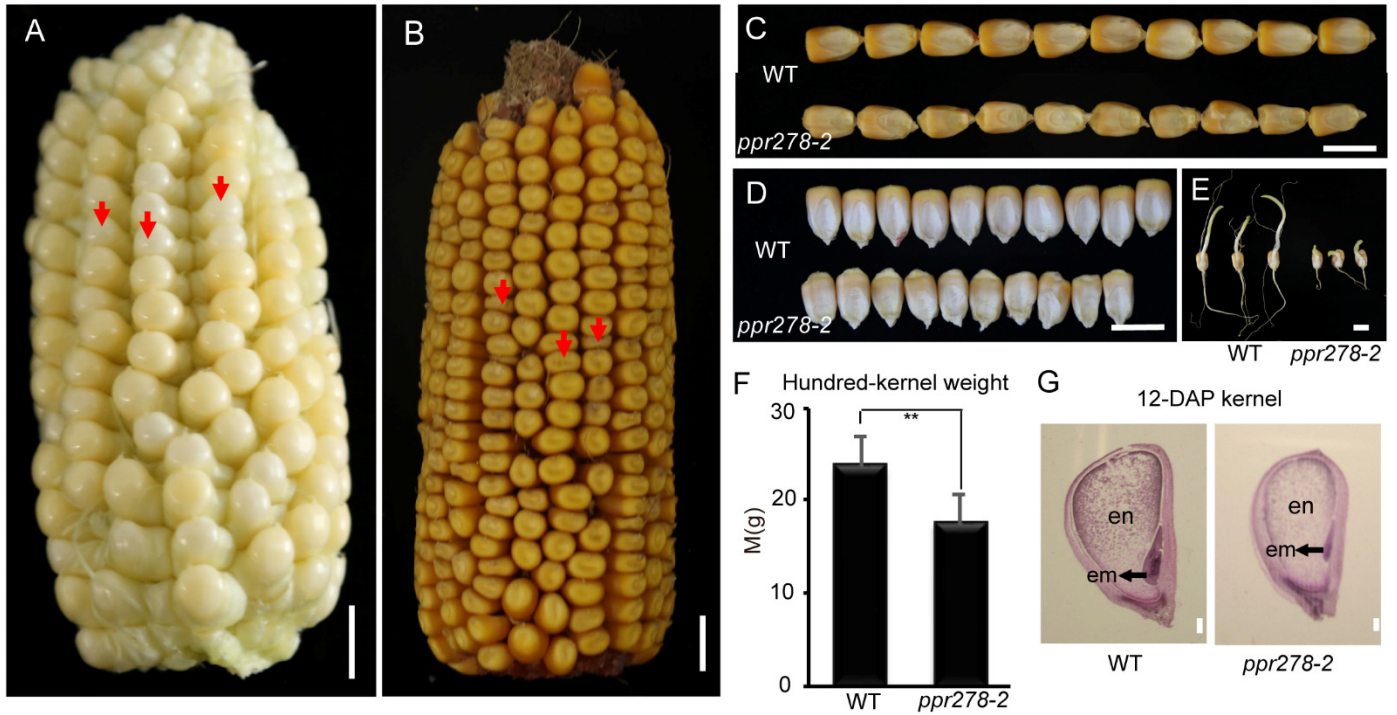


Figure S3. Phenotype of *ppr278-2* mutants was similar to *ppr278-1* mutants. (A,B) Ears of self-pollinated heterozygous *ppr278-2* plants at 16 days after pollination (16 DAP) (A) and at maturity (B). Red arrows indicate the mutant kernels. Bar = 1 cm. (C,D) Comparison of the length (C) and width (D) of mature seeds between the WT and the *ppr278-2* mutant. Bar = 1 cm. (E). Germination of WT and *ppr278-2* mutant seeds after dark culture for 2 days in an incubator. Bar = 1 cm. (F). Comparison of the 100-kernel weight of fully mature WT and mutant *ppr278-2* plants. Values and error bars represent the mean and standard deviation of three biological replicates. ***, $P < 0.001$ (t -test), representing a significant difference. (G). Longitudinal section of WT (left) and *ppr278-2* mutant kernels (right) at 12 DAP. en: endosperm, em: embryo. Bar = 0.5 mm.

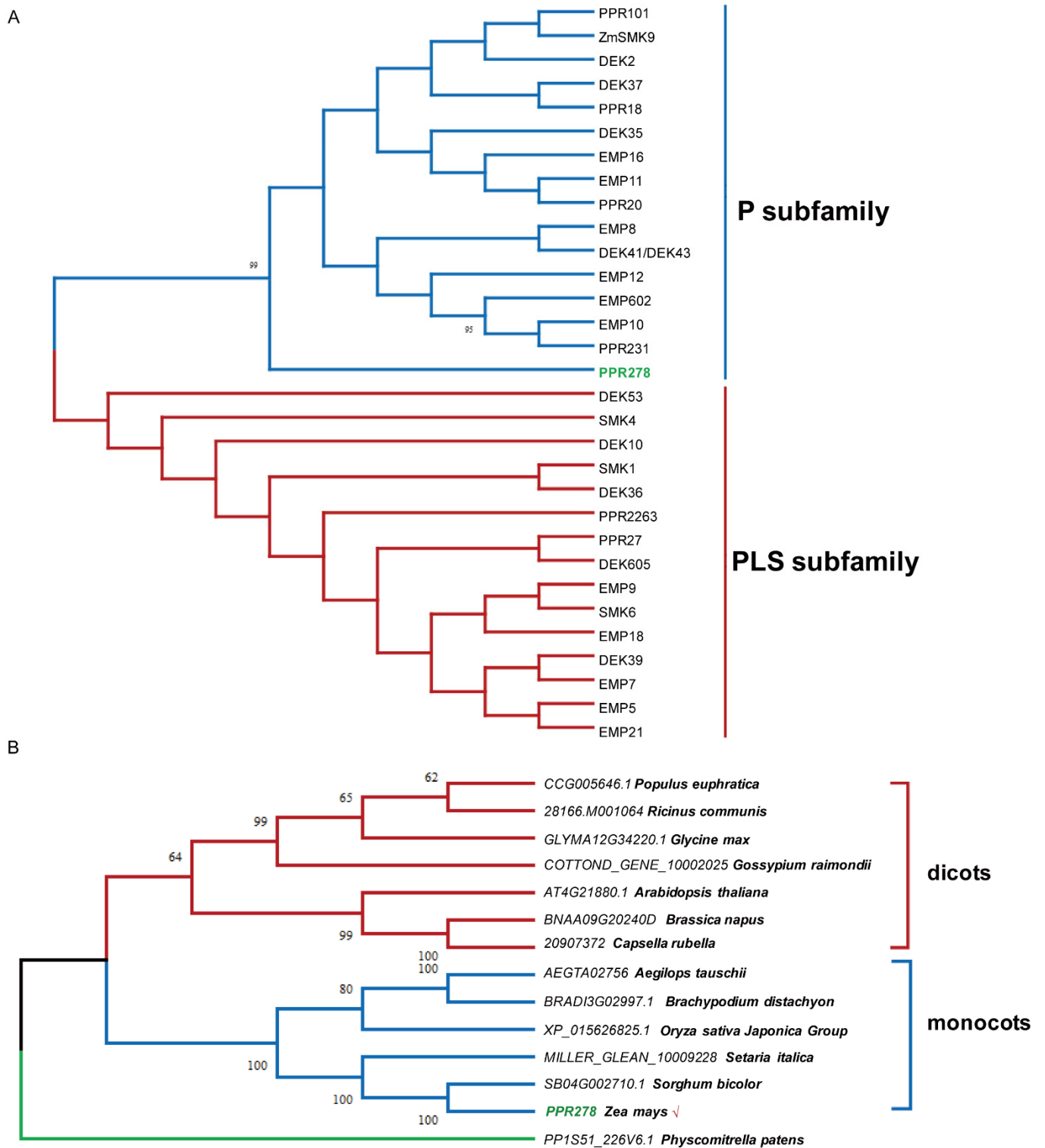


Figure S4. Phylogenetic analysis of PPR278. Phylogenetic analysis of PPR278 protein with published PPR members in maize (**A**) and with homologs in other species (**B**).

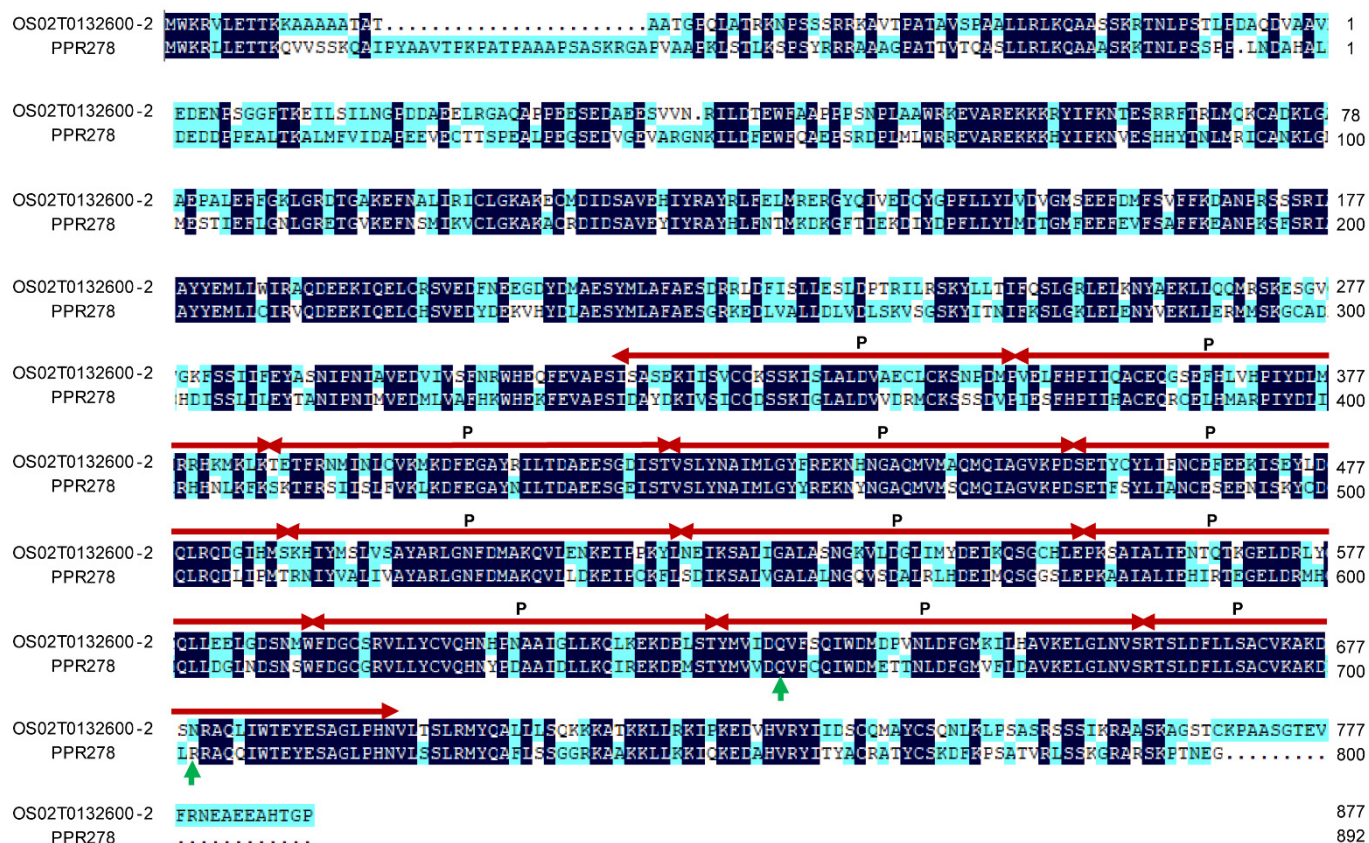


Figure S5. Amino acid sequence alignment of PPR278. Alignment of the amino acid sequence of PPR278 and a putative homolog in rice. Dual red arrows represent the P motifs, and green arrows represent mutant sites.

motif 1: 439-473 IDAYDKIVSICC..DSSKIGLALDVVDRMCKSSSDVP
motif 2: 474-508 IESFHPPIIHACE..QRCELHMARPIYDLIRHHNLKFK
motif 3: 509-543 SKTFRSIIISLFV..KLKDFEGAYNILTDAEESGEIST
motif 4: 544-578 VSLYNAIMLGYY..REKNYNGAQMVMSQMCIAGVKPD
motif 5: 579-610 SETFSYLIANCE..SEENISKYCDQLRQDLIPMT...
motif 6: 611-644 RNIYVALIVAYA..RLGNFDMKQVLLDKEIPCKFL.
motif 7: 645-679 SDIKSALVGALA..LNGQVSDALRLHDEIMQSGGSLE
motif 8: 680-712 PKAAIALIEHIR..TEGELDRMHQLLDGLNDSNSW..
motif 9: 713-747 FDGCGRVLLYCV..QHNYPDAAIDLLKQIREKDEMST
motif 10: 748-784 YMVVDQVFCQIWDMETTNLDGFMVFLDAVKELGLNV
motif 11: 785-819 RTSLDLFLSACV..KAKDLRRAQQIWTIEYESAGLPHN

Figure S6. PPR278 contains 11 atypical P motifs. Amino acid sequence alignment of the P motifs in PPR278. The conserved amino acids are shaded greenish-blue.

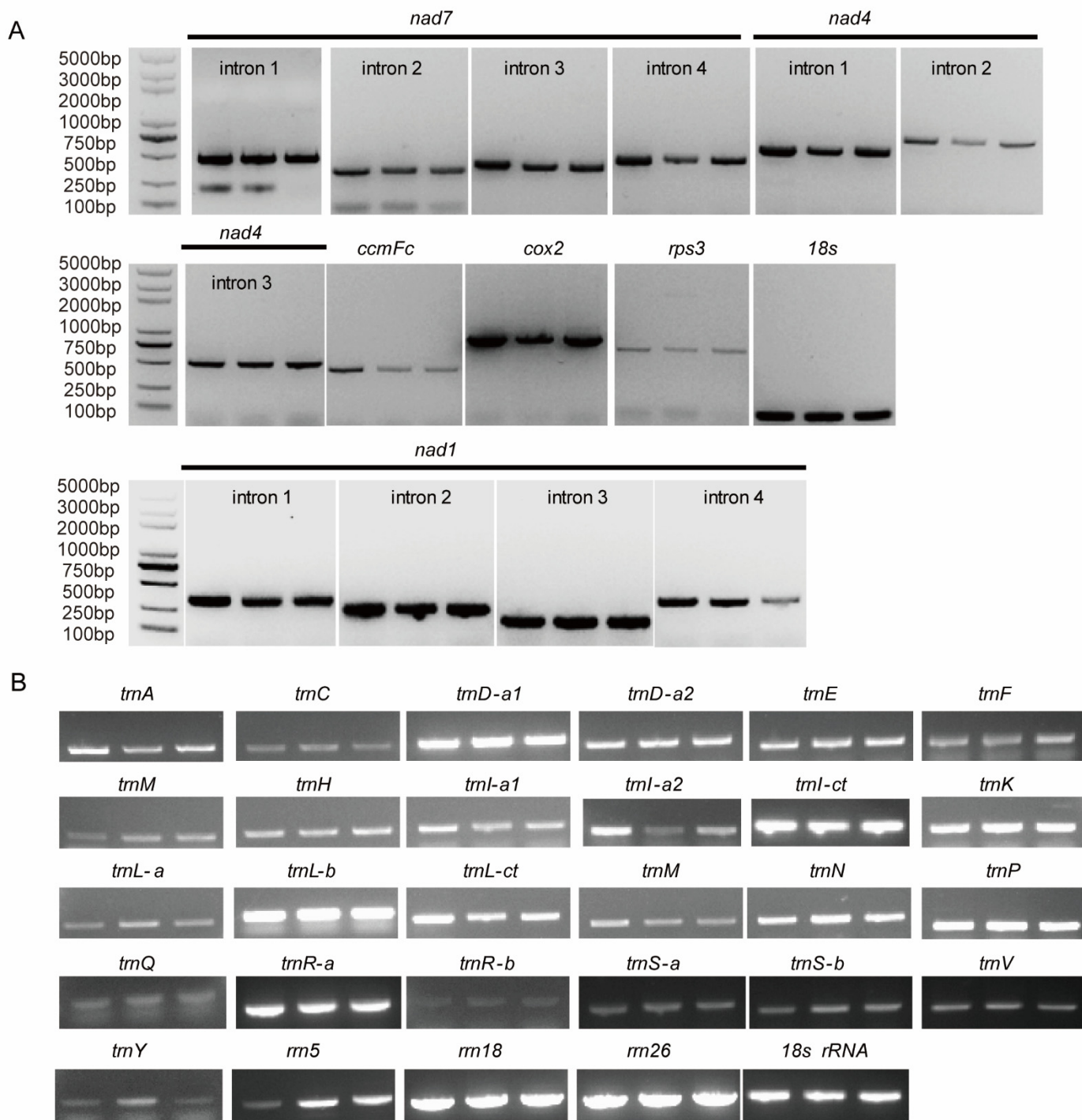


Figure S7. RT-PCR analysis of mitochondrial genes. **(A)** RT-PCR analysis of other group II genes except *nad2* and *nad5* intron splicing efficiency in WT, *ppr278-1* and *ppr278-2* respectively. **(B)** Comparison of mitochondrial tRNAs and rRNAs levels between WT and *ppr278* by RT-PCR. Every lane from the left to right represents WT, *ppr278-1*, *ppr278-2* respectively. A DNA marker is shown in the farther left lane.

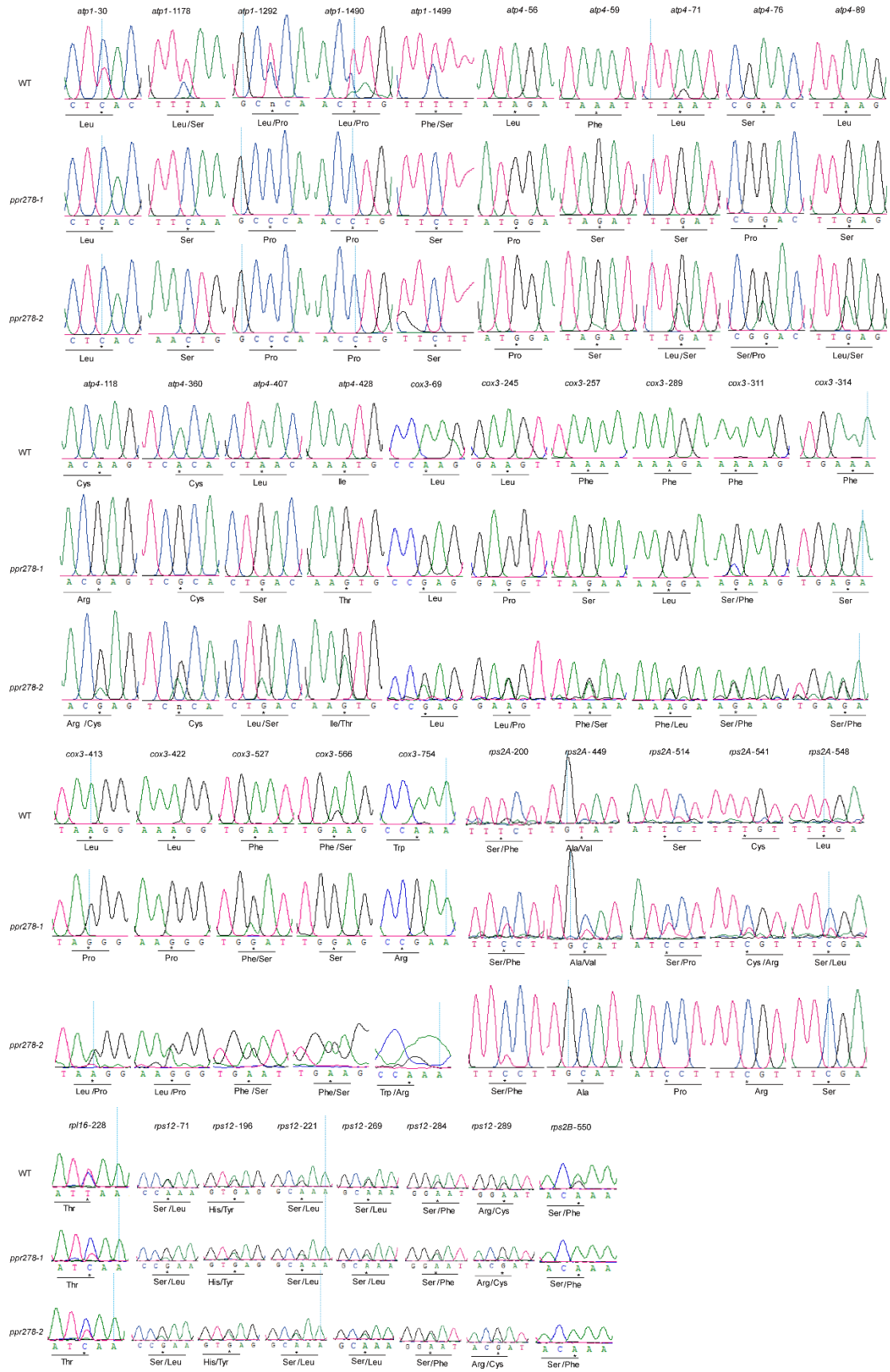


Figure S8. Direct comparison of C-to-U RNA editing sites in mitochondrial genes *atp1*, *atp4*, *cox3*, *rps2A*, *rps2B*, *rps12* and *rpl16* in WT and *ppr278* plants. "n" stands for the peak of heterozygous genotype (C/U) in the same editing site. "*" stands for the C-to-U editing site.

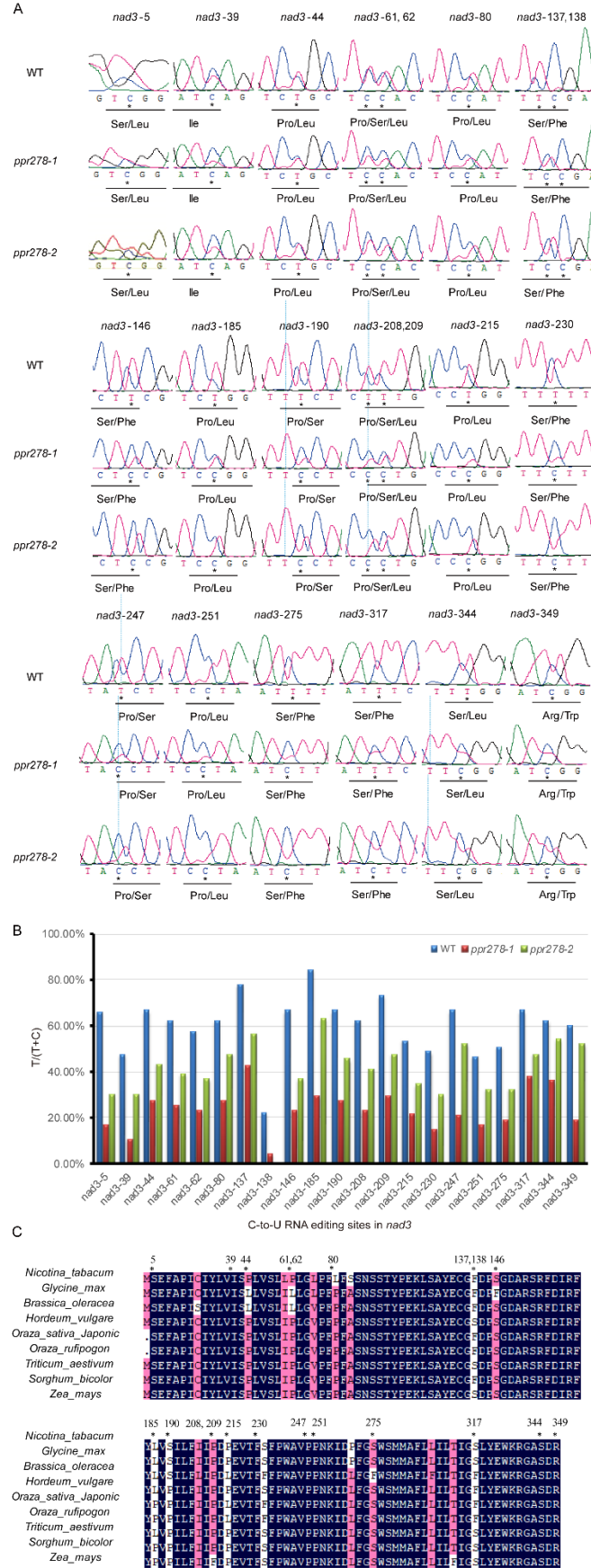


Figure S9. Decreased RNA editing efficiency of *nad3* transcripts in the *ppr278* mutant. **(A)** Direct comparison of C-to-U RNA editing sites in *nad3* in WT and *ppr278* plants. **(B)** Statistics of C-to-U RNA editing efficiency. **(C)** Alignment of *nad3* amino acid sequences in different species. “*” stands for the C-to-U editing site.

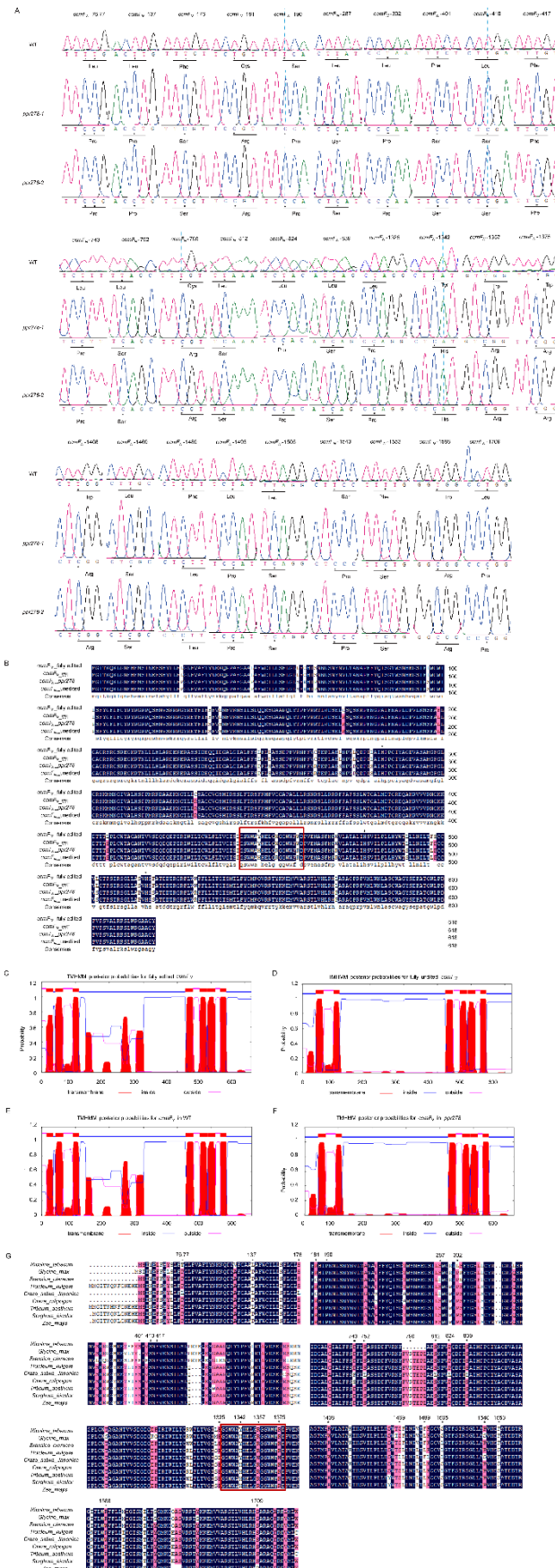


Figure S10. Abolished RNA editing of *ccmFN* transcripts in the *ppr278* mutants. (A) Direct comparison of C-to-U RNA editing sites in *ccmFN* in WT and *ppr278* plants. (B) Comparison of different C-to-U editing states in *ccmFN*. The white or red background represents amino acids substitution sites in *ccmFN*, the red rectangle represents the WWD domain, and the stars represent the conserved

histidines (His). (C–F) The predicted transmembrane domain of different C-to-U RNA editing states of *ccmFN*. (C–D) All C-to-U RNA editing sites are fully edited (C) and unedited (D). (E–F). Two kinds of editing states in WT (E) and *prr278* (F) plants. (G) Alignment of *ccmFN* amino acid sequences in different species. “n” stands for the peak of heterozygous genotype (C/U) in the same editing site. “*” stands for the C-to-U editing site.

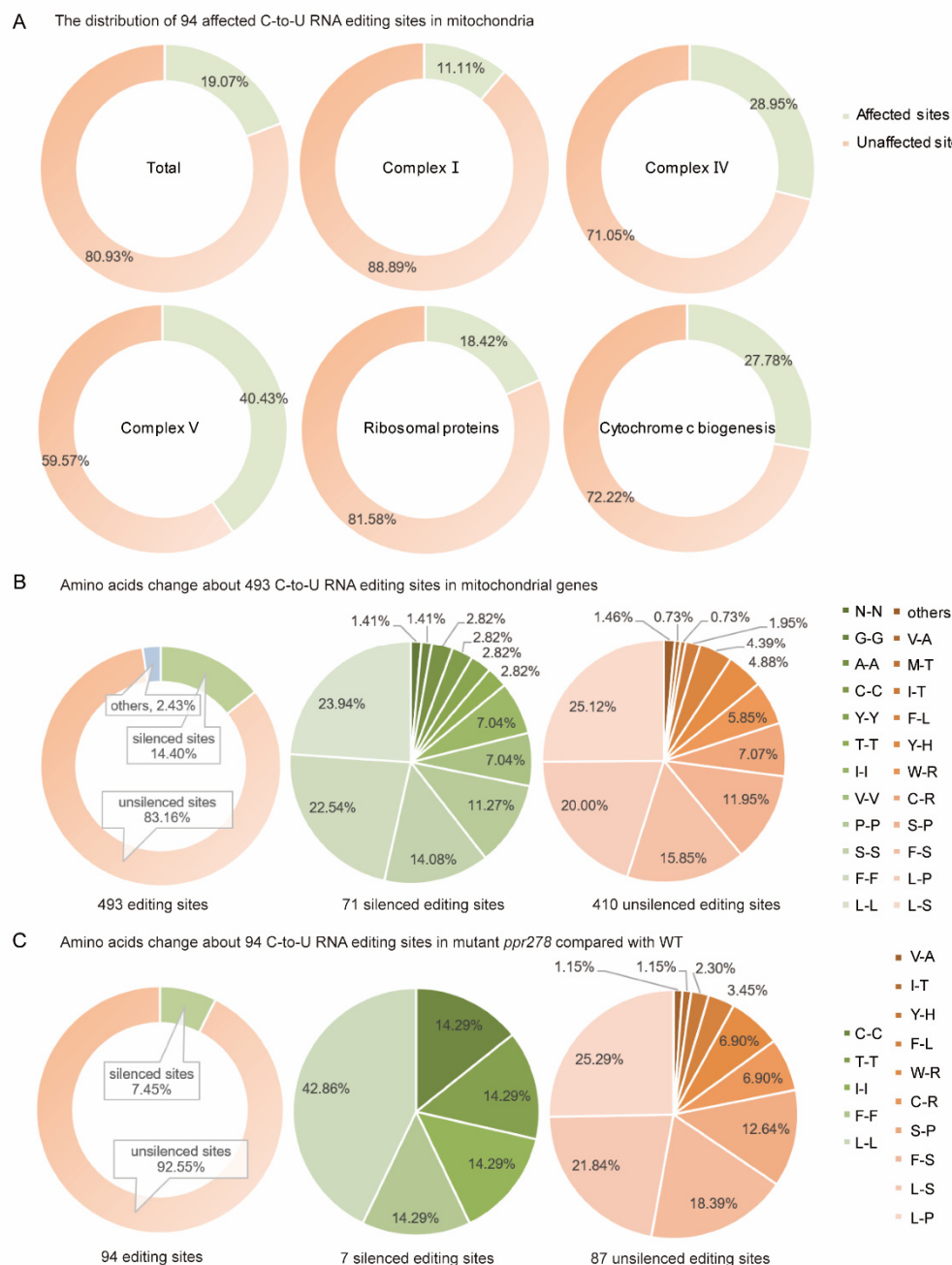


Figure S11. Analysis of amino acid changes related to C-to-U RNA editing of mitochondrial genes. (A) The percentage of C-to-U RNA editing in 94 affected sites in the mitochondria genome, complex I, IV, and V, cytochrome *c* biogenesis, and ribosomal proteins. (B) Amino acid changes at 493 C-to-U RNA editing sites in the mitochondrial genome. “Other” means that C-to-U editing events occurred in untranslated regions. Silenced sites mean that no amino acid change occurred after C-to-U editing. Every pie chart from the left to right represents the statistics of 493 editing sites, 71 silenced sites, and 410 unsilenced sites. (C) Amino acid changes at 94 C-to-U RNA editing sites from fully edited to fully unedited states. Every pie chart from the left to right represents the statistics of 94 affected editing sites, 7 silenced sites, and 87 unsilenced sites. 0.